

Cite this: *Chem. Sci.*, 2022, 13, 8088

All publication charges for this article have been paid for by the Royal Society of Chemistry

Received 31st March 2022
Accepted 1st June 2022

DOI: 10.1039/d2sc01870e

rsc.li/chemical-science

Carbon dioxide reduction by an Al–O–P frustrated Lewis pair†

Lucas Wickemeyer,^a Niklas Aders,^a Andreas Mix,^a Beate Neumann,^a Hans-Georg Stammler,^a Jorge J. Cabrera-Trujillo,^b Israel Fernández^b and Norbert W. Mitzel^{a*}

The reaction of $t\text{Bu}_2\text{P}(\text{O})\text{H}$ with Bis_2AlH ($\text{Bis} = \text{CH}(\text{SiMe}_3)_2$) afforded the adduct $t\text{Bu}_2\text{P}(\text{H})\text{--O--Al}(\text{H})\text{Bis}_2$ (**3**). It slowly releases H_2 to form the first oxygen-bridged geminal Al/P frustrated Lewis pair $t\text{Bu}_2\text{P--O--AlBis}_2$. It is capable of reversibly binding molecular hydrogen to afford **3**, shown by NMR and H/D scrambling experiments, and forms a 1,2-adduct with CO_2 . Importantly, the H_2 adduct **3** reduces CO_2 in a stoichiometric reaction leading to the formic acid adduct $t\text{Bu}_2\text{P}(\text{H})\text{--O--Al}(\text{CO}_2\text{H})\text{Bis}_2$. The formation of the different species was explored by density functional theory calculations which provide support for the experimental results. All products were characterized by NMR spectroscopy as well as X-ray diffraction experiments and elemental analyses.

Introduction

The persisting high level of interest in small molecule activation with frustrated Lewis pairs (FLPs) has led to an enormous variety of different combinations of acid and base functions, the chemistry and applications of which have been investigated in detail.¹ Most typically, boranes with electronegative C_6F_5 substituents are used as Lewis acids.

Among the most intensely studied reactions of FLP are the activation of molecular hydrogen and carbon dioxide or a combination of both, that is a reduction of carbon dioxide. This was achieved with different systems containing boron compounds as Lewis acids.^{2–5} One early example for this is the system $\text{TMP/B}(\text{C}_6\text{F}_5)_3$ ($\text{TMP} = 2,2,6,6\text{-tetramethylpiperidine}$), which cleaves molecular hydrogen to form $[\text{TMP--H}]^+[\text{H--B}(\text{C}_6\text{F}_5)_3]^-$.⁶ This ammonium borate complex reduces CO_2 to the formate stage when used in equimolar amounts and to methanol when used in excess.^{1c}

Despite its intrinsically higher Lewis acidity⁷ the higher homologue aluminum was significantly less frequently used. FLP systems containing aluminum demonstrated their great potential through the large variety of reaction types,⁸ including

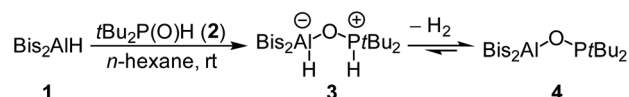
C–H activation,^{9,10} hydrogen activation,¹¹ and carbon dioxide reduction¹² or fixation,^{10,13} as well as their use as catalysts for polymerization reactions.¹⁴ A convenient method to prepare geminal Al/P FLPs is the hydroalumination of alkynylphosphines. The obtained products tend to quench themselves by dimerization or the formation of adducts with the alane reagent, even though it was shown that dimeric species are also able to form adducts with CO_2 .¹⁵

Geminal linker motifs other than carbon-based ones like alkylidene^{10,16} or methylene¹⁷ are rarely found for neutral group 13/P FLP. Köster *et al.* described the formation of different P–O–B species from reactions of diphenylphosphine oxide with trialkylboranes or dialkylhydridoboranes as early as 1987. However, they did not explicitly investigate adduct formations in the sense of FLP chemistry but only reported adducts with an additional hydridodialkylborane being coordinated to the phosphorus atom.¹⁸ Only very recently were a few examples of neutral oxygen-bridged P–O–B systems presented, which show typical reactivity towards CO_2 and molecular hydrogen. However, these reactions require untypically harsh conditions or only reversibly form adducts despite the strongly electronegative substituents at boron.^{19,20} Other reactivities of oxygen-bridged FLP include the reversible binding of SO_2 by a P/B system derived from phosphinoboranes and the activation of B–

^aLehrstuhl für Anorganische Chemie und Strukturchemie, Centrum für Molekulare Materialien CM₂, Fakultät für Chemie, Universität Bielefeld, Universitätsstraße 25, Bielefeld 33615, Germany. E-mail: mitzel@uni-bielefeld.de

^bDepartamento de Química Orgánica I, Centro de Innovación en Química Avanzada (ORFEO-CINQA), Facultad de Ciencias Químicas, Universidad Complutense de Madrid, Madrid 28040, Spain

† Electronic supplementary information (ESI) available: NMR spectra, crystallographic data and computational details. CCDC 2151906–2151909. For ESI and crystallographic data in CIF or other electronic format see <https://doi.org/10.1039/d2sc01870e>



Scheme 1 Synthesis of FLP **4** and reversible formation of the H_2 adduct **3**.

H and O–H bonds by an N/B FLP which is formed in the reaction of TEMPO with $\text{HB}(\text{C}_6\text{F}_5)_2$.²¹

Results and discussion

Synthesis and solid-state structure

We now synthesized the first geminal oxygen-bridged Al/P FLP using the sterically extremely demanding hydridoalane Bis_2AlH ($\text{Bis} = \text{CH}(\text{SiMe}_3)_2$) (**1**) and $t\text{Bu}_2\text{P}(\text{O})\text{H}$ (**2**). Initially they form the phosphane–alane adduct $t\text{Bu}_2\text{P}(\text{H})\text{–O–Al}(\text{H})\text{Bis}_2$ (**3**). This compound then slowly releases H_2 to give the geminal FLP $t\text{Bu}_2\text{P–O–AlBis}_2$ **4** in quantitative yield (Scheme 1).

The NMR spectra show the formation of compound **3** to be completed immediately after mixing the substances. A doublet at 5.76 ppm in the ^1H NMR spectrum shows a characteristic P–H coupling constant of 457 Hz. The $^{31}\text{P}\{^1\text{H}\}$ NMR spectrum contains a signal at 72.6 ppm. The conversion of **3** into **4** under release of hydrogen is rather slow. It was monitored by NMR in a closed tube and is not completed even after two days (conversion of about 92%). Complete conversion to **4** is achieved by removal of all volatiles *in vacuo*. The $^{31}\text{P}\{^1\text{H}\}$ NMR spectrum of **4** shows a singlet at 142.8 ppm; this corresponds well to the comparable P–O–B system $t\text{Bu}_2\text{P–O–Bcat}$ (159.3 ppm).²⁰ Resonances of the methine protons of the $\text{CH}(\text{SiMe}_3)_2$ groups are very sensitive to the coordination number at aluminum; the signal for **4** at -0.38 ppm is in a typical range for tri-coordinated aluminum.²²

The determination of the solid-state structure by single-crystal X-ray diffraction confirms the monomeric structure of **4** (Fig. 1). The molecular structure exhibits a large $\text{Al}(1)\text{–O}(1)\text{–P}(1)$ angle of $138.1(1)^\circ$ and an $\text{Al}(1)\cdots\text{P}(1)$ distance of $3.122(1)$ Å. The aluminum atom features a slightly distorted trigonal-planar coordination with $\text{O}(1)\text{–Al}(1)\text{–C}(1/2)$ angles of $117.6(1)^\circ/127.7(1)^\circ$ and a $\text{C}(1)\text{–Al}(1)\text{–C}(2)$ angle of $114.6(1)^\circ$. The $\text{P}(1)\text{–O}(1)$

bond ($1.635(1)$ Å) is clearly longer than the P–O bond in $t\text{Bu}_2\text{P}(\text{O})\text{H}$ ($1.482(2)$ Å).²³

Reactivity towards hydrogen and carbon dioxide

Strikingly, H/D-scrambling experiments with H_2/D_2 mixtures at one atmosphere of pressure showed a reversible binding of molecular hydrogen to **4**. However, this reaction is rather slow under the given conditions. At first, the formation of small amounts of H_2 and D_2 adducts of **4** was observed after five days. Another week later, the characteristic triplet for HD was observed in the ^1H NMR spectrum at 4.57 ppm with a $^1J_{\text{D,H}}$ coupling constant of 42.6 Hz. Density Functional Theory (DFT) calculations (PCM(hexane)-M06-2X/def2-TZVPP//PCM(hexane)-M06-2X/def2-SVP) confirmed for this binding of hydrogen a free energy difference between **3** and **4** + H_2 of only 1.6 kcal mol^{−1} (at 298 K), with **3** being the more energetically favorable species (Fig. 2). Considering a possible error in this number of a few kcal mol^{−1}, it is consistent with the experimental observation of a slow and incomplete formation of **4** in

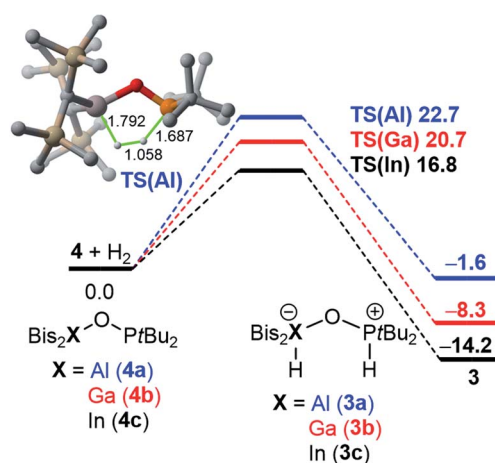


Fig. 2 Computed reaction profile for the interconversion of **3** into **4** + H_2 . Relative free energies (ΔG , at 298 K) and bond lengths (hydrogen atoms are omitted) are given in kcal mol^{−1} and Å, respectively. All data have been computed at the PCM(hexane)-M06-2X/def2-TZVPP//PCM(hexane)-M06-2X/def2-SVP level.

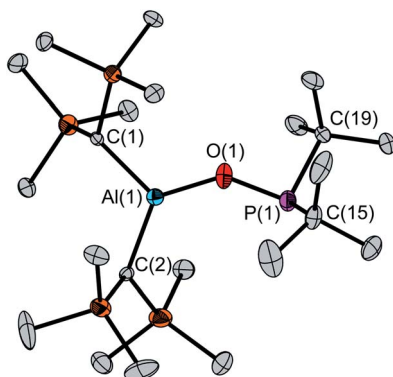
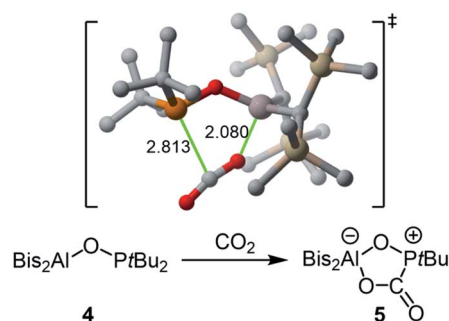


Fig. 1 Molecular structure of **4** in the solid state. Hydrogen atoms and a disordered molecule (occupancy 7%) are omitted for clarity. Ellipsoids are set at 50% probability. Selected distances [Å] and angles [$^\circ$]: $\text{P}(1)\text{–O}(1)$ 1.635(1), $\text{P}(1)\text{–C}(15)$ 1.890(4), $\text{P}(1)\text{–C}(19)$ 1.874(3), $\text{Al}(1)\text{–O}(1)$ 1.708(1), $\text{Al}(1)\text{–C}(1)$ 1.939(3), $\text{Al}(1)\text{–C}(2)$ 1.954(2), $\text{P}(1)\cdots\text{Al}(1)$ 3.122(1); $\text{O}(1)\text{–P}(1)\text{–C}(15)$ 101.4(1), $\text{O}(1)\text{–P}(1)\text{–C}(19)$ 99.2(1), $\text{C}(1)\text{–P}(1)\text{–C}(15)$ 109.4(2), $\text{O}(1)\text{–Al}(1)\text{–C}(1)$ 117.6(1), $\text{O}(1)\text{–Al}(1)\text{–C}(2)$ 127.7(1), $\text{C}(1)\text{–Al}(1)\text{–C}(2)$ 114.6(1), $\text{P}(1)\text{–O}(1)\text{–Al}(1)$ 138.1(1).



Scheme 2 Reaction of FLP **4** with carbon dioxide to form adduct **5** and above the computed transition state (bond lengths are given in Å; hydrogen atoms are omitted for clarity).



the presence of hydrogen. This equilibrium indicates a reversible nature of this process and finds its confirmation by the computed interconversion barrier of $\Delta G^\ddagger = 24.3 \text{ kcal mol}^{-1}$ (from 3).

Interestingly, compared to the analogous systems containing the heavier elements of group 13, gallium and indium, the hydrogen adducts **3_b/c** are thermodynamically favored and the barriers for the reactions **4_b/c** + H₂ → **3_b/c** are lower for the heavier FLPs.

The reaction of **4** with carbon dioxide afforded adduct **5** in nearly quantitative yield (Scheme 2). Unlike in previously reported P–O–B systems, the binding is stable at room temperature and an equilibrium is not formed.^{19,20} Compared to the free FLP **4**, the ³¹P NMR signal at 64.8 ppm is clearly high field shifted, while the characteristic ¹³C{¹H} NMR doublet for the bound CO₂ appears at 166.0 ppm with a ¹J_{P,C} coupling constant of 98.6 Hz. According to our DFT calculations, the formation of **5** occurs in a concerted manner through the asynchronous transition state depicted in Scheme 2²⁴ and with an activation barrier of only 5.5 kcal mol^{−1} in a highly exergonic ($\Delta G_R = -22.9 \text{ kcal mol}^{-1}$) transformation.

The molecular structure of **5** in the crystal shows the formation of a typical planar five-membered ring with an exocyclic C–O moiety (Fig. 3). Its P–O bond at 1.540(2) Å is significantly shorter than in the free FLP **4** (1.635(1) Å) while the Al–O bond is longer at 1.855(2) Å (**4**: 1.708(1) Å). With 117.1(1)° the P(1)–O(1)–Al(1) angle is noticeably narrower than in **4** (138.1(1)°). The sum of angles at C(1) of 360.0(2)° indicates trigonal planar coordination.

CO₂ reduction

The formation of the CO₂ adduct **5** in combination with the reversible binding of molecular hydrogen raised the question of how H₂ adduct **3** would react with CO₂. Since **3** releases hydrogen slowly and is only formed in small amounts when **4** is

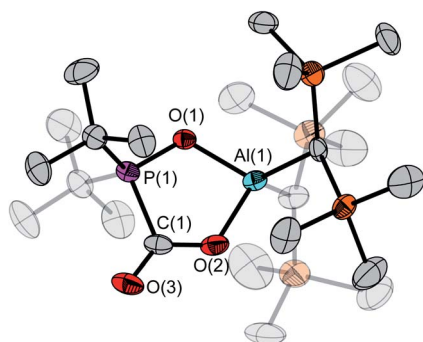
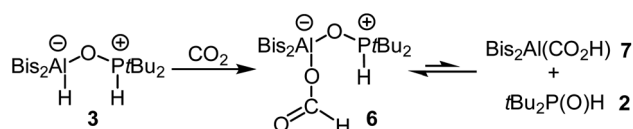


Fig. 3 Molecular structure of the CO₂ adduct **5** in the solid state. Ellipsoids are set at 30% probability. Hydrogen atoms as well as the minor occupied disordered part of the –CH(Si(CH₃)₃)₂ groups are omitted for clarity. Selected bond lengths, distances [Å] and angles [°]: P(1)–O(1) 1.540(2), P(1)–C(1) 1.868(2), Al(1)–O(1) 1.855(2), Al(1)–O(2) 1.848(2), O(2)–C(1) 1.278(3), O(3)–C(1) 1.215(3), P(1)–Al(1) 2.901(1); P(1)–O(1)–Al(1) 117.1(1), O(1)–P(1)–C(1) 101.3(1), C(1)–O(2)–Al(1) 122.0(1), O(2)–C(1)–P(1) 109.6(2), O(3)–C(1)–P(1) 122.8(2), O(3)–C(1)–O(2) 127.6(2).



Scheme 3 Reduction of CO₂ with **3** to form the formic acid adduct **6** and its equilibrium with alane **7** and tBu₂P(O)H (**2**).

treated with hydrogen, handling is only possible for a very limited time. We therefore mixed alane **1** and phosphine **2** to generate **3** which could be reacted directly before the release of hydrogen. Upon complete dissolution of the solids, this mixture was cooled to −196 °C, and the reaction flask was degassed and backfilled with CO₂. By this, we achieved stoichiometric reduction of carbon dioxide to afford the formic acid adduct **6** (Scheme 3). The characteristic ¹H NMR signal for the formate moiety appears at 8.45 ppm, while the ³¹P{¹H} NMR shift of 72.2 ppm is similar to that of **3**. This unexpected reactivity makes FLP **4** a versatile tool with highly useful abilities. Being able to (reversibly) bind both CO₂ and H₂ individually on one hand and at the same time unite both reactivities to reduce carbon dioxide with previously activated molecular hydrogen almost instantly at ambient temperature and atmospheric pressure is a unique combination in the field of FLP chemistry. As mentioned in the introduction, this reactivity has been observed for boron containing systems before. However, the reduction was only achieved at higher temperatures or elevated CO₂ pressure.^{1c,2–5} However, the nature of the individual reactions of **3** with H₂ (equilibrium on the side of free H₂) and CO₂ (formation of a stable adduct) make the system unlikely to be used as a catalyst for the reduction of CO₂.

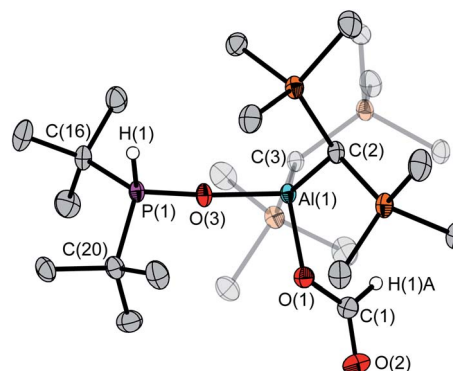


Fig. 4 Molecular structure of **6** in the crystalline state. Only one of two independent molecules in the asymmetric unit is shown. H(1) was refined isotropically while H(1A) was taken into account using a riding model; all other hydrogen atoms were omitted for clarity. Ellipsoids are set at 50% probability. Selected bond lengths [Å] and angles [°]: P(1)–O(3) 1.519(1); P(1)–H(1) 1.278(1), P(1)–C(16) 1.838(1), P(1)–C(20) 1.828(1), Al(1)–O(1) 1.810(1), Al(1)–O(3) 1.814(1), O(1)–C(1) 1.295(1), O(2)–C(1) 1.210(2); O(3)–P(1)–C(16) 111.6(1), O(3)–P(1)–C(20) 109.0(1), C(20)–P(1)–C(16) 117.0(1), P(1)–O(3)–Al(1) 168.8(1), O(1)–Al(1)–O(3) 99.3(1), O(1)–Al(1)–C(2) 108.6(1), O(1)–Al(1)–C(3) 110.2(1), C(1)–O(1)–Al(1) 127.4(1), O(2)–C(1)–O(1) 125.8(1).



Compound **6** forms an equilibrium in solution: small amounts of phosphine **2** and the alane $\text{Bis}_2\text{Al}(\text{CO}_2\text{H})$ (**7**) are observed by NMR spectroscopy (Scheme 3). Characteristic ^1H resonances are the doublet at 5.84 ppm for **2** and the signal of the formate group of **7** at 7.35 ppm.

The asymmetric unit of the unit cell of crystalline **6** contains two independent molecules, whose structural parameters differ mainly in the O–Al–O–P torsion angles ($107.6(3)^\circ/41.6(12)^\circ$); the Al–O–P angles ($168.8(1)^\circ/154.3(1)^\circ$) are noticeably wider than in **4**. Moreover, the bond of aluminum to the bridging oxygen atom is significantly longer ($1.834(1)/1.814(1)$ vs. $1.708(1)$ Å) while the corresponding P–O bond is shorter ($1.529(1)/1.519(1)$ Å vs. $1.635(1)$ Å). The aluminum atom exhibits a slightly distorted tetrahedral geometry, with a τ_4 parameter²⁵ of 0.93 (Fig. 4).

We observed that the formic acid adduct **6** is in equilibrium with small amounts of phosphine oxide **2** and alane **7** in solution. This raised the question of whether CO_2 could also be directly reduced with Bis_2AlH and then treated with $t\text{Bu}_2\text{P}(\text{O})\text{H}$ to give **6**. When alane **1** was reacted directly with CO_2 , the ^1H NMR spectrum of the dissolved solid obtained (**7d**, identified by XRD, see below) contained two sets of signals, those of the monomer **7** and dimer **7d**. Signals for the formate protons are found at 8.84 (**7d**) and 7.33 ppm (**7**). After several days, practically only one species (7.33 ppm, **7**) remained observable. Inconsistent with this experimental observations, the DFT calculations predict the dimerization of **7** to **7d** to be rather exergonic ($\Delta G_R = -19.8$ kcal mol^{−1}).

The identification of these species is based on diffusion ordered spectroscopy (DOSY). Using the Stokes–Einstein equation, the diffusion coefficients of 4.65×10^{-10} m² s^{−1} (8.84 ppm, **7d**) and 5.70×10^{-10} m² s^{−1} (7.33 ppm, **7**) were converted into hydrodynamic radii and volumes: 7.21 Å/ 1570 Å³ for **7d** and 5.87 Å/ 850 Å³ for **7**. Compared to the empirically calculated values²⁶ of 6.29 Å/ 1043 Å³ and 5.01 Å/ 527 Å³, the values in solution are increased due to a solvation shell. Still, the volume of the species at 8.84 ppm is about twice the size of the one at 7.33 ppm, which confirms that monomeric alane **7** forms from an initially dimeric species **7d** upon dissolution (Scheme 4).

Solely the dimeric species was found in the solid state, as determined by X-ray diffraction studies of a single crystal (Fig. 5). It has an almost planar eight-membered ring with an inversion center. Each aluminum atom is coordinated by two oxygen atoms from different formate groups in a distorted tetrahedral manner ($\tau_4 = 0.84$). The Al–O distances differ only slightly at $1.848(1)$ and $1.837(1)$ Å, and so do the C–O distances ($1.255(2)$, $1.239(2)$ Å). In contrast, two very different Al–O–C angles are found at $138.4(1)^\circ$ and $167.9(1)^\circ$.

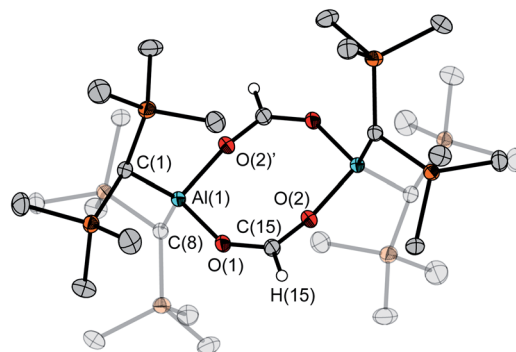


Fig. 5 Molecular structure of **7d** in the crystal. Ellipsoids are set at 50% probability; hydrogen atoms except for the ones of the formate units are omitted for clarity. Selected bond lengths [Å] and angles [°]: Al(1)–O(1) $1.848(1)$, Al(1)–O(2') $1.837(1)$, O(1)–C(15) $1.255(2)$, O(2)–C(15) $1.239(2)$; O(2')–Al(1)–O(1) $99.9(1)$, C(15)–O(1)–Al(1) $138.3(1)$, C(15)–O(2)–Al(1') $167.9(1)$.

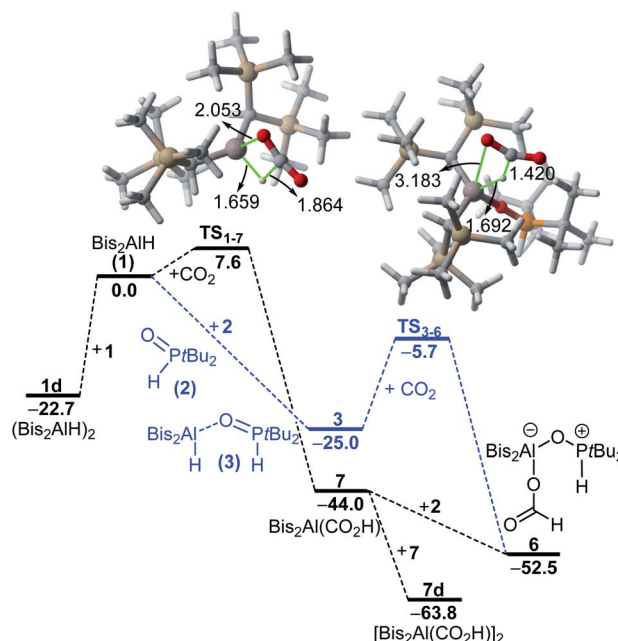
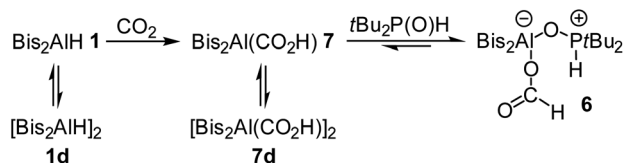


Fig. 6 Computed reaction profiles for the formation of the formic acid adduct **6**. Relative free energies (at 298 K) are given in kcal mol^{−1}, bond lengths in Å. All data have been computed at the PCM(hexane)-M06-2X/def2-TZVPP//PCM(hexane)-M06-2X/def2-SVP level.



Scheme 4 Reduction of CO_2 by Bis_2AlH , equilibria between monomeric and dimeric alanes and formation of formic acid adduct **6**.

When adding phosphine oxide **2** to a solution of $\text{Bis}_2\text{Al}(\text{CO}_2\text{H})$ (**7**), the formic acid adduct **6** is formed. However, as described above, the reaction remains incomplete, and small amounts of phosphine oxide **2** and alane **7** are detectable in solution, which further confirms the proposed equilibrium described above. DFT calculations were also carried out to gain more insight into the formation of **6** in solution (Fig. 6). We found that **1** and **2** form adduct **3** in a barrier-free and highly exergonic reaction ($\Delta G_R = -25.0$ kcal mol^{−1}). Subsequent reaction of **3** with CO_2 leads to the highly exergonic ($\Delta G_R = -27.0$ kcal mol^{−1}) formation of the formic acid adduct **6** via the

transition state **TS**₃₋₆, a saddle point mainly associated with the nucleophilic addition of the aluminum-hydride to the electrophilic carbon atom of CO₂. Both the computed free energy of reaction and activation barrier ($\Delta G^\ddagger = 19.3 \text{ kcal mol}^{-1}$) are compatible with a process occurring at room temperature.

The alternative process involving the initial reaction of alane **1** with CO₂ was also explored. This transformation leads to the exergonic ($\Delta G_R = -44.0 \text{ kcal mol}^{-1}$) formation of **7** with a low activation barrier of only $7.6 \text{ kcal mol}^{-1}$ through the transition state **TS**₁₋₇, a saddle point associated again with the concomitant formation of the new C–H and Al–O bonds. Subsequent barrier-free addition of phosphine oxide **2** leads to the formation of **6** again in an exergonic transformation ($\Delta G_R = -8.5 \text{ kcal mol}^{-1}$).

The computed free energies of reaction and relatively low barriers therefore confirm the feasibility of both alternative processes, the formic acid adduct **6** being the most stable species in both computed profiles. Our calculations also predict that the possible release of formic acid from **6** is highly endergonic ($\Delta G_R = +29.2 \text{ kcal mol}^{-1}$) and thus highly unlikely (see Fig. S19 in the ESI†).

Conclusions

In essence, we have described herein the preparation, full characterization and reactivity of a first geminal oxygen-bridged Al/P FLP *t*Bu₂P–O–AlBis₂. The reactivity of this system includes the reversible binding of molecular hydrogen and adduct formation with carbon dioxide. Reduction of carbon dioxide was achieved with the FLP–H₂ addition product to the formate stage. Its reactivity is unique in the sense of being able to both, to reversibly split molecular hydrogen and to reduce carbon dioxide to the formate stage, with the H₂ addition product rapidly at ambient temperature and atmospheric pressure. Our findings encourage us to further explore and investigate this reactivity. Theoretical results for analogous systems involving the heavier elements gallium and indium indicate the possibility of a facilitated uptake of hydrogen by a higher homologue of FLP **4**. We also expect an easier release of formic acid from the higher homologues of **6**. With this promising outlook we will focus on synthesizing these systems and confirming theoretical predictions with the aim to eventually achieve a catalytic reduction of carbon dioxide.

Experimental section

General considerations

All reactions and manipulations with air- and moisture-sensitive compounds were carried out under conventional Schlenk techniques using nitrogen as inert gas or in a glove box using argon as inert gas. Volatile compounds were handled using a vacuum line. *n*-Hexane and [D₆]benzene were dried over a Na/K alloy, distilled and degassed prior to use. CDCl₃ was dried over 3 Å molecular sieves, distilled and degassed prior to use. CO₂ (99.5%, Linde) was used without further purification. Bis₂AlH (Bis = CH(SiMe₃)₂) was prepared according to a literature procedure.²² NMR spectra were recorded using a Bruker

Avance III 300, Avance III 500 or Avance III 500 HD spectrometer at ambient temperature. Chemical shifts were referenced to the residual proton or carbon signal of the solvent (C₆D₆: ¹H: 7.16 ppm, ¹³C: 128.1 ppm; CDCl₃: ¹H: 7.26 ppm) or externally (²⁹Si: SiMe₄, ³¹P: 85% H₃PO₄ in H₂O). Elemental analyses were carried out by co-workers of the University of Bielefeld using a EURO EA Elemental Analyzer.

Synthetic procedures

Synthesis of *t*Bu₂P(O)H (2). Di-*tert*-butylphosphine oxide was prepared according to a modified literature protocol.²⁷ Di-*tert*-butylchlorophosphine (3.00 g, 16.6 mmol) was dissolved in dichloromethane (15 mL) and degassed water (0.30 g, 17 mmol, 1 eq.) was added at 0 °C. The solution was stirred overnight, and all volatiles were removed *in vacuo*. The residue was redissolved in dichloromethane (20 mL) and washed with saturated sodium hydrogencarbonate solution multiple times (20 mL altogether) until no gas formation was observed. After removal of the solvent, di-*tert*-butylphosphine oxide was obtained as a colorless solid (2.20 g, 13.6 mmol, 82%). The NMR signals were slightly shifted compared to literature values.

Analytical data. ¹H NMR (500 MHz, C₆D₆): δ [ppm] = 5.85 (d, ¹*J*_{P,H} = 419.3 Hz, 1H, P–H), 1.00 (d, ³*J*_{P,H} = 14.5 Hz, 18H, *t*Bu). ³¹P{¹H} NMR (202 MHz, CDCl₃): δ [ppm] = 61.6 Hz. ¹H NMR (500 MHz, CDCl₃): δ [ppm] = 6.06 (d, ¹*J*_{P,H} = 428.6 Hz, 1H, P–H), 1.26 (d, ³*J*_{P,H} = 15.1 Hz, 18H, *t*Bu). ³¹P{¹H} NMR (202 MHz, CDCl₃): δ [ppm] = 66.6 Hz.

Preparation of *t*Bu₂P(H)(O)Al(H)Bis₂ (3). Di-*tert*-butylphosphine oxide (13 mg, 80 mmol) and bis(bis(trimethylsilyl)methyl) alane (28 mg, 81 μmol, 1 eq.) were placed in a Young NMR tube and the reaction monitored *via* NMR spectroscopy.

Analytical data. ¹H NMR (500 MHz, C₆D₆): δ [ppm] = 5.76 (d, ¹*J*_{P,H} = 457.0 Hz, 1H, P–H), 4.58 (br s, 1H, Al–H), 0.83 (d, ³*J*_{P,H} = 16.5 Hz, 18H, *t*Bu), 0.50 (s, 18H, CH(Si(CH₃)₃)₂), 0.43 (s, 18H, CH(Si(CH₃)₃)₂), –1.04 (s, 2H, CH(Si(CH₃)₃)₂). ³¹P{¹H} NMR (202 MHz, C₆D₆): δ [ppm] = 72.6 Hz.

Preparation of *t*Bu₂P(O)AlBis₂ (4). Di-*tert*-butylphosphine oxide (138 mg, 851 μmol) and bis(bis(trimethylsilyl)methyl) alane (295 mg, 851 μmol, 1 eq.) were placed in an ampoule fitted with a greaseless tap. *n*-Hexane (5 mL) was added at room temperature and the solution was stirred overnight. All volatiles were removed *in vacuo* and *t*Bu₂P(O)AlBis₂ was obtained as a colorless solid (424 mg, 836 μmol, 98%). Crystals were obtained by slowly evaporating a solution of *t*Bu₂P(O)AlBis₂ in *n*-hexane.

Analytical data. ¹H NMR (300 MHz, C₆D₆): δ [ppm] = 1.20 (d, ³*J*_{P,H} = 10.7 Hz, 18H, C(CH₃)₃), 0.31 (d, 36H, Si(CH₃)₃), –0.38 (s, 2H, CH(SiMe₃)₂). ¹³C{¹H} NMR (75 MHz, C₆D₆): δ [ppm] = 35.0 (d, ¹*J*_{P,C} = 31.7 Hz, C(CH₃)₃), 28.2 (d, ²*J*_{P,C} = 16.0 Hz, C(CH₃)₃), 8.7 (s, CH(Si(CH₃)₃)₂), 4.6 (s, CH(Si(CH₃)₃)₂). ²⁹Si{¹H} NMR (60 MHz, C₆D₆): δ [ppm] = –2.7 (s). ³¹P{¹H} NMR (121 MHz, C₆D₆): δ [ppm] = 142.6 (s). Elemental analysis calcd (%) for C₂₂H₅₆AlO₂Si₄ (*M*_r = 506.98): C 52.12, H 11.13; found: C 52.81, H 11.04.

Preparation of *t*Bu₂P(O)AlBis₂·CO₂ (5). FLP (57 mg, 0.11 mmol) was placed in an ampoule with a greaseless tap and dissolved in *n*-hexane (5 mL). The solution was degassed (1 ×



freeze–pump–thaw) and CO₂ (0.46 mmol, 4.2 eq.) was condensed into the ampoule. The solution was stirred overnight and all volatiles were removed *in vacuo* to obtain FLP·CO₂ as a colorless solid (61 mg, 0.11 mmol, quant.). Crystals were obtained by slow evaporation of a solution of *t*Bu₂P(O)AlBis₂·CO₂ in C₆D₆.

Analytical data. ¹H NMR (500 MHz, C₆D₆): δ [ppm] = 0.99 (d, ³J_{P,H} = 15.7 Hz, 18H, C(CH₃)₃), 0.39 (s, 18H, Si(CH₃)₃), 0.38 (s, 18H, Si(CH₃)₃), −0.79 (br s, 1H, CH(SiMe₃)₂), −1.09 (br s, 1H, CH(SiMe₃)₂). ¹³C{¹H} NMR (126 MHz, C₆D₆): δ [ppm] = 166.0 (d, ¹J_{P,C} = 98.6 Hz, CO₂), 34.8 (d, ¹J_{P,C} = 42.2 Hz, C(CH₃)₃), 26.3 (s, C(CH₃)₃), 5.3 (s, CH(Si(CH₃)₃)₂), 5.1 (s, CH(Si(CH₃)₃)₂), signals of the methine proton were not observed due to high dynamics. ²⁹Si{¹H} NMR (99 MHz, C₆D₆): δ [ppm] = −1.8 (br m). ³¹P{¹H} NMR (202 MHz, C₆D₆): δ [ppm] = 64.8 (s). Elemental analysis calcd (%) for C₂₃H₅₆AlO₃PSi₄ (M_r = 550.99): C 50.14, H 10.24; found: C 50.20, H 10.03.

Preparation of *t*Bu₂P(H)(O)Al(CO₂H)Bis₂ (6). Bis(bis(trimethylsilyl)methyl)alane (139 mg, 401 μmol) and di-*tert*-butylphosphine oxide (65 mg, 0.40 mmol, 1 eq.) were placed in an ampoule with a greaseless tap and *n*-hexane (5 mL) was added. Right after dissolution of all solids, the mixture was frozen with liquid N₂ and evacuated. CO₂ (800 μmol, 2 eq.) was condensed into the ampoule and the mixture was allowed to reach room temperature and stirred overnight. After removal of all volatiles, a colorless oil was obtained, which was recrystallized from *n*-hexane at −5 °C to obtain *t*Bu₂P(H)(O)Al(CO₂H)Bis₂ as colorless crystals (97 mg, 0.18 mmol, 44%). Crystals were obtained by slowly evaporating a solution of *t*Bu₂P(H)(O)Al(CO₂H)Bis₂ in C₆D₆. In solution, the component forms an equilibrium with *t*Bu₂P(O)H and Bis₂Al(CO₂H).

Analytical data. ¹H NMR (500 MHz, C₆D₆): δ [ppm] = 8.45 (s, 1H, CO₂H), 6.50 (d, ¹J_{P,H} = 485.3 Hz, 1H, P-H), 0.88 (d, ³J_{P,H} = 16.6 Hz, 18H, P(C(CH₃)₃)₂), 0.43 (s, 18H, CH(Si(CH₃)₃)₂), 0.39 (s, 18H, CH(Si(CH₃)₃)₂), −1.00 (s, 2H, CH(Si(CH₃)₃)₂). ¹³C{¹H} NMR (126 MHz, C₆D₆): δ [ppm] = 162.6 (s, CO₂H), 33.7 (d, ¹J_{P,C} = 56.1 Hz, C(CH₃)₃), 26.0 (s, C(CH₃)₃), 5.6 (s, CH(Si(CH₃)₃)₂), 5.3 (s, CH(Si(CH₃)₃)₂), 2.4 (br s, CH(Si(CH₃)₃)₂). ²⁹Si{¹H} NMR (99 MHz, C₆D₆): δ [ppm] = −1.2 (s), −2.0 (s). ³¹P{¹H} NMR (121 MHz, C₆D₆): δ [ppm] = 72.3 (s). Elemental analysis calcd (%) for C₂₃H₅₈AlO₃PSi₄ (M_r = 553.01): C 49.95, H 10.57; found: C 50.19, H 10.85.

Preparation of Bis₂Al(CO₂H) (7)/(Bis₂Al(CO₂H))₂ (7d). In an ampoule with a greaseless tap, bis(bis(trimethylsilyl)methyl)alane (105 mg, 303 μmol) was dissolved in *n*-hexane (4 mL) and degassed (1× freeze–pump–thaw). CO₂ (0.61 mmol, 2 eq.) was condensed into the ampoule and the reaction mixture was allowed to reach room temperature, resulting in the formation of a colorless suspension which was stirred overnight. All volatiles were removed *in vacuo* and Bis₂Al(CO₂H) was obtained as a colorless solid (128 mg, 303 μmol, quant.). Crystals were obtained by slow evaporation of a solution of (Bis₂Al(CO₂H))₂ in C₆D₆.

Analytical data. ¹H NMR (500 MHz, C₆D₆): δ [ppm] = 8.84 (s, 2H, CO₂H of 7d), 7.33 (s, 1H, CO₂H), 0.28 (s, 72H, CH(SiCH₃)₂ of 7d), 0.24 (s, 36H, CH(SiCH₃)₂), −0.93 (s, 4H, CH(SiMe₃)₂ of 7d), −1.06 (s, 2H, CH(SiMe₃)₂). ¹³C{¹H} NMR (126 MHz, C₆D₆): δ [ppm] = 170.5 (s, CO₂H of 7d), 166.8 (s, CO₂H), 4.9 (s, CH(SiCH₃)₂ of 7d), 4.8 (s, CH(SiCH₃)₂), 1.8 (s, CH(SiCH₃)₂), 1.5

(s, CH(SiCH₃)₂ of 7d). ²⁹Si{¹H} NMR (99 MHz, C₆D₆): δ [ppm] = −1.6 (s), −1.7 (s, 7d). Elemental analysis calcd (%) for C₁₅H₃₉AlO₂Si₄ (M_r = 390.80): C 46.10, H 10.06; found: C 45.98, H 10.31.

Author contributions

Lucas Wickemeyer: synthesis, spectroscopy, conceptualization, visualization, writing – original draft; Niklas Aders: synthesis of HALBis₂, conceptualization; Beate Neumann and Hans-Georg Stammel: crystallography; Jorge J. Cabrera-Trujillo and Israel Fernández: quantum-chemical calculations, writing – quantum-chemical paragraphs; Norbert W. Mitzel: conceptualization, project administration, supervision, writing – review & editing.

Conflicts of interest

There are no conflicts to declare.

Acknowledgements

We thank Barbara Teichner for performing CHN analyses. The work was funded by the Deutsche Forschungsgemeinschaft (DFG, German Research Foundation) – grant MI 477/44-1, project number 461833739 and the Spanish Ministerio de Ciencia e Innovación/Agencia Estatal de Investigación/10.13039/501100011033 (grants PID2019-106184GB-I00 and RED2018-102387-T).

Notes and references

- (a) T. W. Hudnall, Y.-M. Kim, M. W. P. Bebbington, D. Bourissou and F. P. Gabbaï, *J. Am. Chem. Soc.*, 2008, **130**, 10890; (b) D. W. Stephan, *Dalton Trans.*, 2009, 3129; (c) A. E. Ashley, A. L. Thompson and D. O'Hare, *Angew. Chem., Int. Ed.*, 2009, **48**, 9839; (d) D. W. Stephan and G. Erker, *Angew. Chem., Int. Ed.*, 2010, **49**, 46; (e) D. W. Stephan and G. Erker, *Chem. Sci.*, 2014, **5**, 2625; (f) D. W. Stephan and G. Erker, *Angew. Chem., Int. Ed.*, 2015, **54**, 6400; (g) D. W. Stephan, *Science*, 2016, **354**, aaf7229; (h) A. F. G. Maier, S. Tussing, T. Schneider, U. Flörke, Z.-W. Qu, S. Grimme and J. Paradies, *Angew. Chem., Int. Ed.*, 2016, **55**, 12219; (i) W. Meng, X. Feng and H. Du, *Acc. Chem. Res.*, 2018, **51**, 191; (j) F.-G. Fontaine and É. Rochette, *Acc. Chem. Res.*, 2018, **51**, 454; (k) Q. Sun, C. G. Daniliuc, C. Mück-Lichtenfeld, K. Bergander, G. Kehr and G. Erker, *J. Am. Chem. Soc.*, 2020, **142**, 17260.
- S. D. Tran, T. A. Tronic, W. Kaminsky, D. M. Heinekey and J. M. Mayer, *Inorg. Chim. Acta*, 2011, **369**, 126.
- M.-A. Courtemanche, A. P. Pulis, É. Rochette, M.-A. Légaré, D. W. Stephan and F.-G. Fontaine, *Chem. Commun.*, 2015, **51**, 9797.
- T. Zhao, X. Hu, Y. Wu and Z. Zhang, *Angew. Chem., Int. Ed.*, 2019, **58**, 722.
- T. Wang, M. Xu, A. R. Jupp, Z.-W. Qu, S. Grimme and D. W. Stephan, *Angew. Chem., Int. Ed.*, 2021, **60**, 25771.
- V. Sumerin, F. Schulz, M. Nieger, M. Leskelä, T. Repo and B. Rieger, *Angew. Chem., Int. Ed.*, 2008, **47**, 6001.



- 7 (a) A. Y. Timoshkin and G. Frenking, *Organometallics*, 2008, **27**, 371; (b) J. A. Plumley and J. D. Evanseck, *J. Phys. Chem. A*, 2009, **113**, 5985.
- 8 M. Layh, W. Uhl, G. Bouhadir and D. Bourissou, *Organoaluminum Compounds and Lewis Pairs in Patai's Chemistry of Functional Groups*, ed. Z. Rappoport, Wiley, Chichester, 2016, pp. 1–46.
- 9 (a) M. A. Dureen and D. W. Stephan, *J. Am. Chem. Soc.*, 2009, **131**, 8396; (b) G. Ménard and D. W. Stephan, *Angew. Chem., Int. Ed.*, 2012, **51**, 4409; (c) S. Chen, B. Li, X. Wang, Y. Huang, J. Li, H. Zhu, L. Zhao, G. Frenking and H. W. Roesky, *Chem.–Eur. J.*, 2017, **23**, 13633; (d) Y. Chen, W. Jiang, B. Li, G. Fu, S. Chen and H. Zhu, *Dalton Trans.*, 2019, **48**, 9152.
- 10 C. Appelt, H. Westenberg, F. Bertini, A. W. Ehlers, J. C. Slootweg, K. Lammertsma and W. Uhl, *Angew. Chem., Int. Ed.*, 2011, **50**, 3925.
- 11 (a) G. Ménard and D. W. Stephan, *Angew. Chem., Int. Ed.*, 2012, **51**, 8272; (b) S. Styra, M. Radius, E. Moos, A. Bihlmeier and F. Breher, *Chem.–Eur. J.*, 2016, **22**, 9508; (c) A. Friedrich, J. Eyselein, H. Elsen, J. Langer, J. Pahl, M. Wiesinger and S. Harder, *Chem.–Eur. J.*, 2021, **27**, 7756; (d) J. J. Cabrera-Trujillo and I. Fernández, *Chem.–Eur. J.*, 2018, **24**, 17823.
- 12 (a) G. Ménard and D. W. Stephan, *J. Am. Chem. Soc.*, 2010, **132**, 1796; (b) G. Ménard and D. W. Stephan, *Angew. Chem., Int. Ed.*, 2011, **50**, 8396.
- 13 (a) M.-A. Courtemanche, J. Larouche, M.-A. Légaré, W. Bi, L. Maron and F.-G. Fontaine, *Organometallics*, 2013, **32**, 6804; (b) H. S. Zijlstra, J. Pahl, J. Penafiel and S. Harder, *Dalton Trans.*, 2017, **46**, 3601.
- 14 (a) D. Chakraborty and E. Y.-X. Chen, *Macromolecules*, 2002, **35**, 13; (b) Y. Zhang, G. M. Miyake and E. Y.-X. Chen, *Angew. Chem., Int. Ed.*, 2010, **49**, 10158.
- 15 (a) W. Uhl, C. Appelt, J. Backs, H. Westenberg, A. Wollschläger and J. Tannert, *Organometallics*, 2014, **33**, 1212; (b) H. H. Karsch, A. Appelt, F. H. Köhler and G. Müller, *Organometallics*, 1985, **4**, 231; (c) J. Boudreau, M.-A. Courtemanche and F.-G. Fontaine, *Chem. Commun.*, 2011, **47**, 11131; (d) S. Roters, C. Appelt, H. Westenberg, A. Hepp, J. C. Slootweg, K. Lammertsma and W. Uhl, *Dalton Trans.*, 2012, **41**, 9033.
- 16 (a) C. Rosorius, G. Kehr, R. Fröhlich, S. Grimme and G. Erker, *Organometallics*, 2011, **30**, 4211; (b) J. Backs, M. Lange, J. Possart, A. Wollschläger, C. Mück-Lichtenfeld and W. Uhl, *Angew. Chem., Int. Ed.*, 2017, **56**, 3094.
- 17 (a) A. Schnurr, H. Vitze, M. Bolte, H.-W. Lerner and M. Wagner, *Organometallics*, 2010, **29**, 6012; (b) X. Zhao, T. M. Gilbert and D. W. Stephan, *Chem.–Eur. J.*, 2010, **16**, 10304; (c) A. Stute, G. Kehr, R. Fröhlich and G. Erker, *Chem. Commun.*, 2011, **47**, 4288; (d) F. Bertini, V. Lyaskovskyy, B. J. J. Timmer, F. J. J. de Kanter, M. Lutz, A. W. Ehlers, J. C. Slootweg and K. Lammertsma, *J. Am. Chem. Soc.*, 2012, **134**, 201.
- 18 R. Köster, Y.-H. Tsay and L. Synoradzki, *Chem. Ber.*, 1987, **120**, 1117.
- 19 Y. Wang, Z. H. Li and H. Wang, *RSC Adv.*, 2018, **8**, 26271.
- 20 D. Zhu, Z.-W. Qu and D. W. Stephan, *Dalton Trans.*, 2020, **49**, 901.
- 21 (a) N. Szykiewicz, J. Chojnacki and R. Grubba, *Inorg. Chem.*, 2020, **59**, 6332; (b) Y. Pan, J. Cui, Y. Wei, Z. Xu and T. Wang, *Dalton Trans.*, 2021, **50**, 8947.
- 22 W. Uhl, L. Cuyper, R. Graupner, J. Molter, A. Vester and B. Neumüller, *Z. Anorg. Allg. Chem.*, 2001, **627**, 607.
- 23 F. Dornhaus, H.-W. Lerner and M. Bolte, *Acta Crystallogr., Sect. E: Crystallogr. Commun.*, 2005, **61**, o657–o658.
- 24 This resembles related transition states associated with the addition of CO₂ to geminal FLPs. See, for instance, ref. 17d and J. J. Cabrera-Trujillo and I. Fernández, *Chem. Commun.*, 2019, **55**, 675.
- 25 A. Okuniewski, D. Rosiak, J. Chojnacki and B. Becker, *Polyhedron*, 2015, **90**, 47.
- 26 Y. H. Zhao, M. H. Abraham and A. M. Zissimos, *J. Org. Chem.*, 2003, **68**, 7368.
- 27 K. A. Smoll, W. Kaminsky and K. I. Goldberg, *Organometallics*, 2017, **36**, 1213.

